Response of a Strongly Eddying Global Ocean to North Atlantic Freshwater Perturbations

MATTHIJS DEN TOOM AND HENK A. DIJKSTRA

Institute for Marine and Atmospheric Research Utrecht, and Department of Physics and Astronomy, Utrecht University, Utrecht, Netherlands

WILBERT WEIJER, MATTHEW W. HECHT, AND MATHEW E. MALTRUD

Los Alamos National Laboratory, Los Alamos, New Mexico

ERIK VAN SEBILLE

Climate Change Research Centre, and ARC Centre of Excellence for Climate System Science, University of New South Wales, Sydney, New South Wales, Australia

(Manuscript received 17 August 2012, in final form 20 October 2013)

ABSTRACT

The strongly eddying version of the Parallel Ocean Program (POP) is used in two 45-yr simulations to investigate the response of the Atlantic meridional overturning circulation (AMOC) to strongly enhanced freshwater input due to Greenland melting, with an integrated flux of 0.5 Sverdrups (Sv; $1\ \text{Sv} \equiv 10^6\ \text{m}^3\ \text{s}^{-1}$). For comparison, a similar set of experiments is performed using a noneddying version of POP. The aim is to identify the signature of the salt advection feedback in the two configurations. For this reason, surface salinity is not restored in these experiments. The freshwater input leads to a quantitatively comparable reduction of the overturning strength in the two models. To examine the importance of transient effects in the relation between AMOC strength and density distribution, the results of the eddy-resolving model are related to water mass transformation theory. The freshwater forcing leads to a reduction of the rate of light to dense water conversion in the North Atlantic, but there is no change in dense to light transformation elsewhere, implying that high density layers are continuously deflating. The main focus of the paper is on the effect of the AMOC reduction on the basinwide advection of freshwater. The low-resolution model results show a change of the net freshwater advection that is consistent with the salt advection feedback. However, for the eddy-resolving model, the net freshwater advection into the Atlantic basin appears to be unaffected, despite the significant change in the large-scale velocity structure.

1. Introduction

Computational resources put constraints on the resolution that can be used for the ocean component of a global climate model (GCM). At the moment, typical horizontal grid spacing for such a model is 1°. This is too coarse to resolve the first baroclinic Rossby radius of deformation, which is a fundamental horizontal scale of mesoscale processes. As a result, the representation of the oceans in a GCM is significantly different from observations in several crucial aspects. For example, the data presented by Bower et al. (2009) show that recently formed deep water follows irregular interior pathways. This provides more detail to the idea that this water flows southward as part of a relatively steady, coherent deep western boundary current, such as is suggested by coarse-resolution ocean models (Drijfhout et al. 1996). The trajectories taken by water parcels are much better represented in a high-resolution, eddy-resolving model (Bower et al. 2009). As a result, low-resolution models may provide incorrect estimates of the ocean's sensitivity to external forcing. In this paper, we address the response of the Atlantic meridional overturning circulation (AMOC) to anomalous high-latitude freshwater forcing.

Corresponding author address: Henk A. Dijkstra, Institute for Marine and Atmospheric Research Utrecht, Dept. of Physics and Astronomy, Utrecht University, Princetonplein 5, 3584 CC Utrecht, Netherlands.
E-mail: h.a.dijkstra@uu.nl

DOI: 10.1175/JPO-D-12-0155.1

Motivation for this study is the results by Weijer et al. (2012), who used the Parallel Ocean Program (POP) in two configurations, with horizontal resolutions of 1° and 0.1°, respectively. It was shown that the transient response to the addition of 0.1 Sverdrups (Sv; $1\,\text{Sv} \equiv 10^6\,\text{m}^3\,\text{s}^{-1}$) of freshwater is significantly different between the two configurations. In the low-resolution version of the model, the AMOC strength levels off after a rapid initial decline, while in the high-resolution configuration, the AMOC decline is more gradual and persistent. In addition, only in the high-resolution configuration is the response found to depend strongly on where the anomalous freshwater forcing is applied. As shown in Weijer et al. (2012), the initial (first 20 yr) decline of the AMOC in these simulations can be related to the behavior of convection, meaning that the efficiency of the anomalous freshwater transport to the sites of convection is an important factor in explaining the differences between the simulations (Marsh et al. 2010). In the present paper, we continue the analysis of Weijer et al. (2012), but instead focus on differences between the two configurations in processes acting at the scale of the basin. Specifically, we frame the discussion around the question of what the signature of the so-called salt advection feedback is in the high-resolution configuration and whether it differs from that in the low-resolution version of the model.

The concept of the salt advection feedback is commonly illustrated with a two-box model, as originally proposed by Stommel (1961). The basic idea is that the overturning is proportional to a meridional density gradient, while, in turn, the overturning enhances the meridional density gradient by reducing the salinity gradient. The temperature advection feedback is commonly assumed to be less important due to the strong damping of temperature anomalies by the atmosphere. Whether the three-dimensional ocean circulation has analogous dynamics is not a simple question. In coarse-resolution ocean–climate models, the salt advection feedback is found to be responsible for the existence of multiple equilibria (Rahmstorf 2000). Hence, abrupt transitions between different states may occur in these models. The possibility of any future transition of the AMOC strongly motivates the study of the response of the AMOC on freshwater perturbations. The results of these studies can also be important for the interpretation of rapid climate changes in the past, the Dansgaard–Oeschger and Heinrich events, as derived from ice-core records (Alley et al. 2003). However, because of computational constraints, the detection of multiple equilibria is currently not feasible for global eddying models.

Quite recently, it has been suggested that the sign of the freshwater transport by the AMOC at 35°S, indicated by M_{ov}, may serve as an indicator of possible multiple states of the AMOC (Rahmstorf 1996; De Vries and Weber 2005; Dijkstra 2007; Huisman et al. 2010; Drijfhout et al. 2011; Hawkins et al. 2011). When M_{ov} is positive in the present-day equilibrium state, the salt advection feedback is stabilizing the AMOC, while when M_{ov} is negative, it means that the salt advection feedback is destabilizing the AMOC. This suggests that M_{ov} is the relevant quantity related to the advective salt transport in the Stommel (1961) box model. Inverse modeling (Weijer et al. 1999) and direct observations (Bryden et al. 2011) suggest that the overturning circulation is exporting freshwater from the Atlantic, that is, $M_{ov} < 0$.

In Huisman et al. (2010), the connection between the transient response of the AMOC to freshwater anomalies and the sign of M_{ov} of the (initial) equilibrium state was investigated. It was found that the impact of the salt advection feedback on the AMOC can already be determined from the transient development of the freshwater budget at 35°S. Therefore, the approach taken in this paper is to examine the connection between the conceptual model of Stommel (1961) and the noneddying and eddy-resolving versions of POP, using transient decadal time-scale simulations of the response to anomalous freshwater forcing.

As anomalous freshwater forcing, we consider enhanced runoff from the Greenland Ice Sheet (GrIS). Observations indicate that the mass balance of the ice sheet is currently negative (Rignot et al. 2011), while future projections suggest that discharge from the GrIS will increase further in the course of the twenty-first century (Mernild et al. 2010). However, our aim is not to provide a realistic GrIS melting scenario but to isolate the oceanic response to a large freshwater perturbation with a realistic pattern. We therefore enhance the amplitude of the GrIS discharge to 0.5 Sv.

Scenarios more relevant for future climate change have been explored extensively in low-resolution models and may be compared to the results with the noneddying version of POP that will be described here. For example, using the Modular Ocean Model (MOM) at a horizontal resolution of about 2°, Gerdes et al. (2006) investigated the role of different ocean–atmosphere boundary conditions in determining the response of the Atlantic to GrIS freshwater anomalies. They show that the strength of the AMOC decreases by about 50% in 100 yr in response to an integrated freshwater perturbation of 0.1 Sv. Furthermore, Stammer (2008) uses the Massachusetts Institute of Technology General Circulation Model (MITgcm) at a horizontal resolution of 1° in a 50-yr simulation with enhanced runoff from Greenland (the integrated flux is not provided). Jungclaus et al. (2006) consider the AMOC change in the ECHAM5-Ocean Model, version 1 (OM1)

(1.5° horizontal circulation in the ocean model), under different scenarios of GrIS melting and greenhouse forcing. For high melting estimates, the AMOC reduction is about 42%, compared to 30% for the Special Report on Emissions Scenarios A1B (SRES-A1B) scenario only. The paper of Hu et al. (2009) considers the effect of enhanced GrIS melting in transient simulations with the Community Climate System Model (CCSM), version 3, under the SRES-A1B scenario. Note that the ocean component of CCSM is POP, which is configured at the same 1° horizontal resolution as considered in this study. In Hu et al. (2009), the AMOC strength decreases by about 50% in 2100, but only when the GrIS melting flux is very strong, being 0.3 Sv in 2100.

A description of the model and the simulations used in this study is given in section 2. The response of the AMOC to the freshwater perturbation is presented in section 3. Section 4 discusses the relation of the AMOC to the meridional density distribution, and in section 5, the role of the AMOC in the freshwater budget of the Atlantic is analyzed. The paper concludes with a summary and discussion in section 6.

2. Model and simulations

The global simulations described here are performed using POP (Dukowicz and Smith 1994), developed at Los Alamos National Laboratory. We consider the same two configurations as Weijer et al. (2012). The strongly eddying configuration, indicated by $R_{0.1}$, has a nominal horizontal resolution of 0.1° and is the same as that used by Maltrud et al. (2010). The low-resolution configuration ($x1$), on the other hand, has the nominal 1° horizontal resolution of CCSM. The two versions of the model are configured to be consistent with each other, where possible. There are, however, some notable differences, which are discussed in full in the supplementary material of Weijer et al. (2012). Here, we note that the $R_{0.1}$ configuration has a tripolar grid layout (Murray 1996) with poles in Canada and Russia, while the $x1$ configuration is based on a grid with two poles, with the northern pole placed onto Greenland. In the $R_{0.1}$ configuration, the model has 42 nonequidistant z levels, increasing in thickness from 10 m just below the upper boundary to 250 m just above the lower boundary at 6000-m depth. In addition, bottom topography is discretized using partial bottom cells, creating a more accurate and smoother representation of topographic slopes. In contrast, in the $x1$ configuration the bottom is placed at 5500-m depth, there are 40 levels (with the same spacing as in $R_{0.1}$), and the partial bottom cell approach is not used.

Since this study focuses on the impact of explicitly resolved mesoscale transports on the decadal response of the global ocean to freshwater flux perturbations, we restrict the time scales introduced by the surface forcing to seasonal. The atmospheric state is based on the repeat annual cycle (normal year) Co-ordinated Ocean–Ice Reference Experiments (CORE; see http://www.clivar.org/wgomd/core/core-1)-forcing dataset (Large and Yeager 2004), with the 6-hourly forcing averaged to monthly. Wind stress is calculated offline using the Hurrell sea surface temperature (SST) climatology (Hurrell et al. 2008) and standard bulk formulae. Evaporation and sensible heat flux are calculated online using bulk formulae and the model predicted SST. Precipitation is also taken from the CORE-forcing dataset. Monthly river runoff from 46 major rivers (Fekete et al. 2000) is added to the freshwater flux at the locations of the actual outflow, with the remaining runoff distributed evenly along the coasts of all of the continents. In the model all freshwater fluxes are converted to equivalent virtual salt fluxes, so that no volume flux is associated with them. In the presentation of our results, though, we refer to these salt fluxes as if freshwater is exchanged across the upper boundary of the model. Ice cover is prescribed based on the −1.8°C isoline of the SST climatology, with both temperature and salinity restored on a time scale of 30 days under diagnosed climatological ice. Consequently, whereas in reality the distribution of sea ice may respond to changes in the surface circulation of the Arctic and subpolar regions, thus modifying the magnitude and pattern of ice–ocean heat and freshwater exchange, this feedback is not represented in the simulations described here.

Our $R_{0.1}$ experiments branch off from the end of year 75 of a simulation spun up from rest, the results of which are described in Maltrud et al. (2010). In this spinup integration global salinity drift was controlled by applying a relaxation condition with a time scale of 1 yr to the surface salinity in the open ocean, additional to the climatological precipitation, (SST dependent) evaporation, and runoff specified above. Because such forcing would artificially remove salinity perturbations (Marsh et al. 2010), the dependence of the salt flux on sea surface salinity is removed in the experiments described here. This is done by diagnosing the salt flux implied by the restoring condition from the next 5 yr (years 76–80) of the spinup simulation and adding the result to the climatological fluxes. The annual-mean field of the total flux is plotted in Fig. 1a and shows a good agreement with observations [e.g., the Hamburg Ocean Atmosphere Parameters and Fluxes from Satellite Data (HOAPS) as in Fig. 16 of Andersson et al. (2010)].

In contrast to the $R_{0.1}$ configuration, in the $x1$ configuration the integrated freshwater budget of the Atlantic and Arctic Oceans (discussed in section 5 below) does

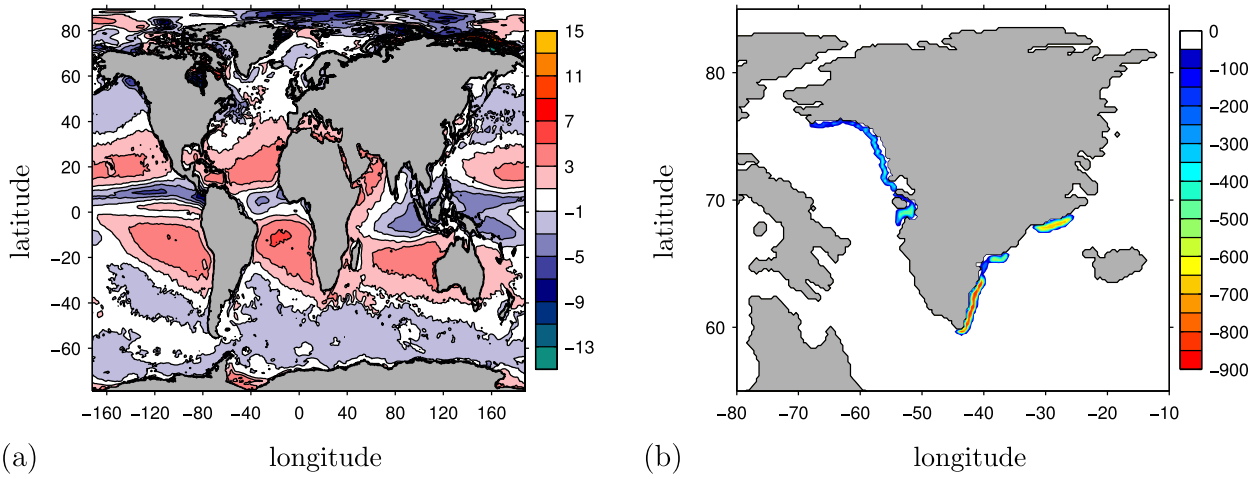

FIG. 1. Annual-mean fields of the seasonally varying virtual salt flux for the $R_{0.1}$ configuration, converted to units of mm day^{-1} with positive values indicating evaporation. (a) Reference flux consisting of climatological evaporation, precipitation, and runoff, plus the diagnosed flux implied by the restoring condition in the spinup integration. Apart from minor changes due to evaporation depending on SST, this flux is constant throughout the years and the same in both simulations studied. This plot shows the field for year 76 in REF. (b) Runoff from Greenland as applied in PERT.

not reach equilibrium within a 75-yr spinup. Therefore, for $x1$ a sufficiently equilibrated state is obtained by integrating the model for an additional 500 yr under mixed boundary conditions. The $x1$ simulations then branch off from this state.

For both configurations, we present the results of two experiments: an unperturbed reference simulation (REF) and an experiment with enhanced runoff from the GrIS (PERT). The REF experiment with the $R_{0.1}$ configuration is also used by Weijer et al. (2012), referred to as C-Mixed in their paper, who present a comparison with observations in the auxiliary material of their paper. The anomalous flux in the PERT simulations is applied throughout the duration of the experiments. Its spatial distribution, shown in Fig. 1b for $R_{0.1}$, is based on observed values of runoff and calving (Rignot and Kanagaratnam 2006). The integrated flux is much larger than observed, however, varying seasonally around an annual-mean amplitude of 0.5 Sv and reaching a maximum amplitude of 0.9 Sv in July. The two simulations are continued for 45 and 100 yr for the $R_{0.1}$ and $x1$ configurations, respectively. For all simulations, monthly-mean data were saved. In addition, daily fields were saved for the years 76 and 116 for the $R_{0.1}$ configuration to allow a better reconstruction of the overturning circulation in density coordinates (discussed in section 4b below).

3. Overturning circulation

A first-order picture of the evolution in the basin-scale overturning circulation is obtained by calculating the meridional overturning streamfunction in depth coordinates, given by

$$\Psi(\phi, z, t) = -r_0 \cos\phi \int_{\lambda_W}^{\lambda_E} \int_{-H}^{z} v(\lambda, \phi, z', t)\, dz'\, d\lambda\,, \qquad (1)$$

where λ is longitude, ϕ is latitude, z is the height above mean sea level, t is time, and r_0 is the radius of Earth. Furthermore, λ_W and λ_E are the (latitude dependent) longitude of the western and eastern boundary of the basin, respectively. Finally, H is the local bottom depth, and $v(\lambda, \phi, z', t)$ is the meridional velocity.

First, the results for the $x1$ simulations are described. Figure 2a shows the maximum value of Ψ at 26.5°N, which is the latitude of the Rapid Climate Change (RAPID) observational array (Cunningham et al. 2007). For the control simulation (REF), the mean is 21 Sv, which is somewhat stronger than the observations suggest. The root-mean-square deviation is 1.7 Sv, which is clearly smaller than what is observed (±6 Sv). Note that the annual variance is constant in time, as mechanisms introducing interannual variability (e.g., through the forcing or internal instabilities) are not represented in the $x1$ version of the model.

The transient response of the AMOC to the freshwater perturbation (PERT) is characterized by a rapid decline in the first 8 yr, followed by a slight resumption up to year 11, after which the decrease continues until the end of the simulation. After 45 yr (the duration of the $R_{0.1}$ simulations), the AMOC has weakened by 8.5 Sv. Even 100 yr after the onset of the perturbation,

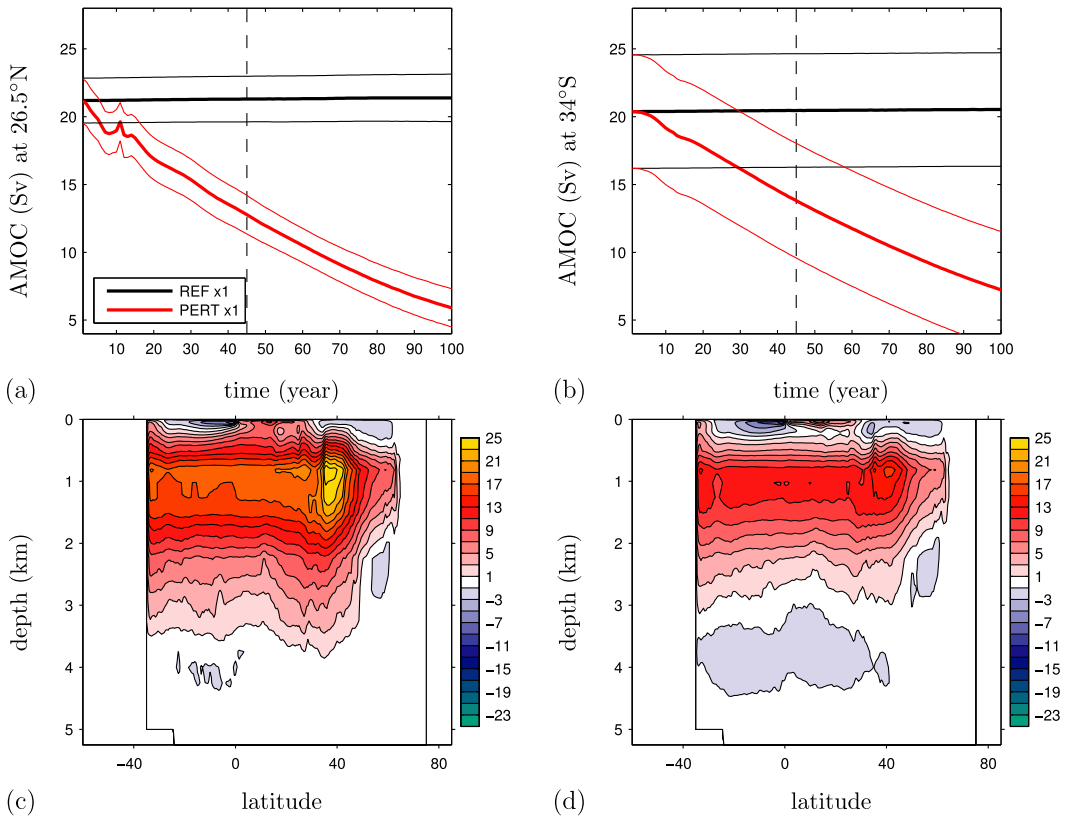

FIG. 2. The AMOC for the $x1$ POP configuration. (top) AMOC strength at (a) 26.5°N and (b) 34°S, diagnosed as the maximum value of Ψ [Eq. (1)], which occurs at the depth of about 1 km. In this and subsequent time series plots, the thick lines are annual-mean values, while the thin lines represent the ±1-yr root-mean-square deviations. The dashed line drawn at 45 yr indicates the duration of the corresponding $R_{0.1}$ simulations. (bottom) Stream functions (contour interval 2 Sv) of the annual-mean AMOC in PERT for year (c) 1 and (d) 41.

the AMOC strength is still decreasing. The decline of the AMOC strength is a meridionally coherent signal (Figs. 2b–d). As a result, it affects the basinwide divergence of freshwater transport, as will be discussed in section 5.

Next, we discuss the results for the $R_{0.1}$ configuration. The strength of the Ψ at 26.5°N is plotted in Fig. 3a. Comparison with Fig. 2 shows that the average strength of the AMOC in the REF case (22 Sv) is similar to that in the $x1$ configuration. The typical 1-yr root-mean square deviation (about 1.5 Sv) is also comparable. Although a long-term adjustment to a quasi-equilibrium situation may still be underway, most of the year-to-year variations must be attributed to intrinsic variability. Note here that the surface forcing does not introduce time scales longer than 1 yr. Because part of the short-term variability is removed by using monthly-averaged forcing, it is not surprising that the AMOC variability is still much larger in the observations (±6 Sv; Cunningham et al. 2007) than in the highly eddying version of the model.

In the $R_{0.1}$ PERT simulation, the AMOC strength shows a small decrease in the first 3 yr after the onset of the freshwater perturbation, attaining an annual-mean value below the weakest annual-mean strength in REF in year 78. Only after about 2 decades, however, is there a persistent, gradual decline in overturning strength, resulting in an anomaly with respect to the REF experiment that clearly exceeds the intra-annual variations. A precise explanation of what determines the timing of the response is outside the scope of this paper. We note, however, that AMOC variations propagate at the Kelvin wave speed south of 34°N, but at the much slower advection speed north of that latitude. As a result there is at least a 6-yr time lag between variations in Labrador Sea mixed layer depth and AMOC variations at 26.5°N (Zhang 2010). In addition, the access of the freshwater anomalies to the sites of deep convection is limited by the narrow boundary currents in the basin (Marsh et al. 2010; Weijer et al. 2012). The year 120 anomaly of the annual-mean strength equals −10.4 Sv, exceeding the response in the $x1$ configuration by about

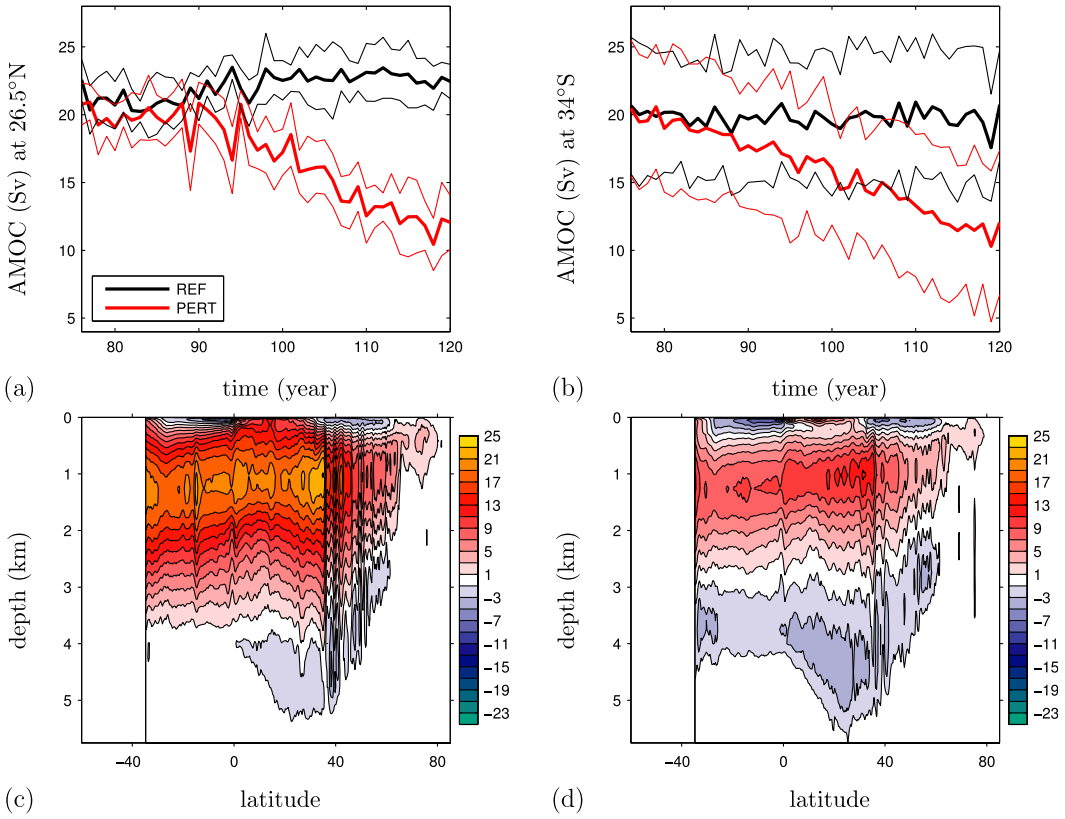

FIG. 3. As in Fig. 2, but for the $R_{0.1}$ POP configuration and year (c) 76 and (d) 116.

2 Sv. Furthermore, the anomaly is about 50% larger than the anomaly in the equivalent simulation with a 0.1-Sv integrated input of freshwater described by Weijer et al. (2012).

As will be discussed in section 5, changes in the AMOC strength are expected to affect the transport of freshwater at the southern margin of the Atlantic at 34°S. Figures 2b and 3b show that for both resolutions, and for both experiments, the annual-mean strength of the AMOC at 34°S is similar to that at 26.5°N, although intra-annual variability is larger. We further note that the year-to-year variations in the $R_{0.1}$ case are smaller at 34°S. In PERT, the AMOC strength decreases almost linearly in $R_{0.1}$, first reaching an annual-mean value lower than that seen in REF in year 89.

Comparison of Figs. 3c and 3d shows that there is no change in the depth of maximum overturning between year 76 and year 116 of the PERT experiment. This is also true for the minimum of the streamfunction at 4.5-km depth, representing northward bottom flow, although the strength of this negative cell increases by roughly 2 Sv between year 76 and year 116. For the $x1$ simulation (Figs. 2c,d), the pattern also does not change. For both cases, the rate of overturning has changed, but the pattern of Ψ is essentially not modified during the simulation, which suggests that the AMOC does not experience a transition (collapse) to a different state. The integration period is, however, quite short, and it is possible that when the simulation would be continued that the AMOC would eventually collapse.

4. AMOC strength and density distribution

To investigate how to connect Stommel (1961)'s conceptual model of the salt advection feedback to the three-dimensional ocean circulation, as represented here by the noneddying and eddying versions of POP, we consider in this section the relation between AMOC strength and the Atlantic density distribution.

a. Relation between AMOC and meridional density contrast

As reviewed by, for example, Rahmstorf (1996) and De Boer et al. (2010), theoretical scaling relations indicate that the AMOC is driven by a meridional density contrast. Although counterexamples are provided by De Boer et al. (2010), there are several model results that indeed show a positive relation between the AMOC

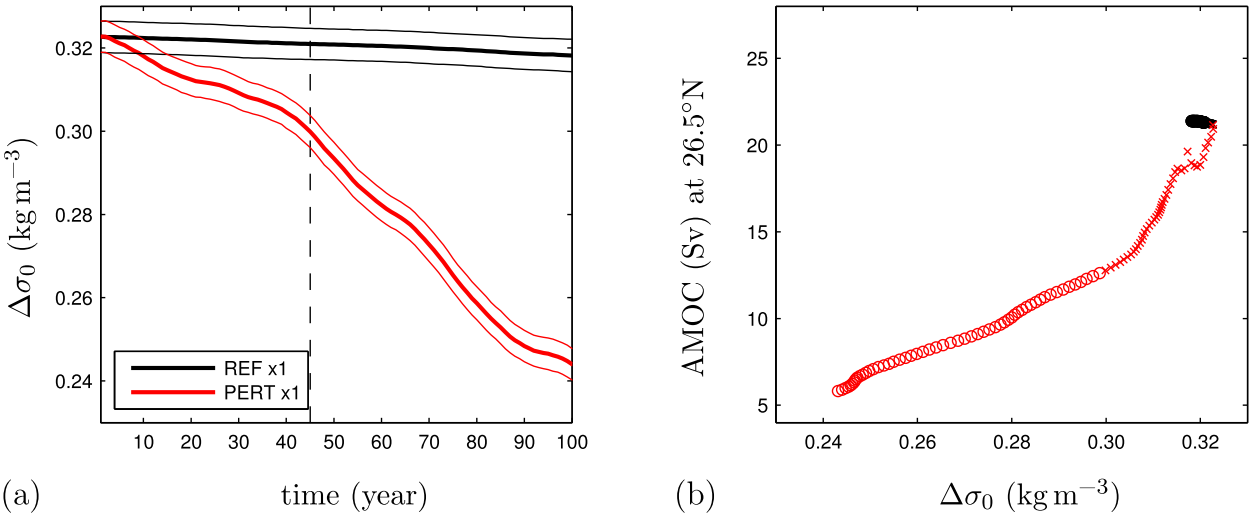

FIG. 4. (a) Time series of the meridional density difference $\Delta\sigma_0$ for the $x1$ configuration. The figure shows the difference in potential density (referenced to the surface) between two latitudinal strips [50°–55°N and 35°–40°S; as in Rahmstorf (1996)] at a model level depth of 918 m. (b) Relation between AMOC strength at 26.5°N and $\Delta\sigma_0$, based on yearly means. Crosses (×) indicate values from years 1–45, while circles (○) indicate values from years 46–100. Similar relations hold for other latitudinal ranges and for other depths.

strength and meridional density contrast (Rahmstorf 1996; Dijkstra 2008) or meridional pressure difference (Griesel and Maqueda 2006). The theoretical relations are based on the assumption of steady-state conditions, while we apply the concept to transient model results. However, rather than establishing the validity of the scaling relation, we want to test whether the salt advection feedback is involved in the response of the AMOC. For this to be true, a positive relation between AMOC strength and meridional density contrast must also hold on the time scale of the simulations described here. Note that in the conceptual model of Stommel (1961), the dependence of the flow strength on the meridional density difference is expressed by a diagnostic relation.

We present here the meridional potential density contrast ($\Delta\sigma_0$, referenced to the surface) at a depth of 918 m, where the difference is taken between the latitudinal strips 50°–55°N and 35°–40°S, as in Rahmstorf (1996). Figure 4a shows that $\Delta\sigma_0$ reduces in response to the freshwater perturbation. When plotted against Ψ, a positive correlation is evident (Fig. 4b), although the relation is clearly not linear. Obviously, the positive correlation does not imply causality, but the result is at least consistent with the flow law used in Stommel (1961)'s model. This is, however, not the case for the $R_{0.1}$ POP model. In Fig. 5a, it is shown that in PERT the density difference $\Delta\sigma_0$ even increases in time and becomes larger than that of REF. This may seem at odds with the fact that a freshwater perturbation is applied in the North Atlantic, which should lead to a density reduction. It is, however, caused by densities decreasing faster in the southern strip than in the northern strip. For PERT, a correlation holds between $\Delta\sigma_0$ and the AMOC strength, but it is opposite to that found in the $x1$ version of the model (Fig. 5b). A similar conclusion is reached based on the computation of meridional density differences at different depths and on meridional pressure differences as in Griesel and Maqueda (2006).

b. *Watermass transformation theory*

The approach taken in the above provides no information about the importance of transient effects for the relation between surface densities and the evolution of the AMOC. We therefore continue the analysis for the strongly eddying model simulations by relating the results to water mass transformation theory (Walin 1982; Marsh et al. 2000).

In this analysis, we use the isopycnal overturning streamfunction, defined as

$$\psi(\phi, b, t) = -r_0 \cos\phi \int_{\lambda_W}^{\lambda_E} \int_{-H}^{\zeta(\lambda,\phi,b,t)} v(\lambda, \phi, z, t)\, dz\, d\lambda\,. \quad (2)$$

Here, b represents a buoyancy variable, and $\zeta(\lambda, \phi, b, t)$ is the height of the surface with buoyancy b. In our analysis potential density referenced to 2000 m is used, that is, $b = \sigma_2$. In contrast to the evaluation of the depth coordinate streamfunction Ψ [Eq. (1)], monthly-averaged data are not sufficient to construct ψ, due to the time dependence of the upper limit of integration ζ. We therefore restrict the analysis in this subsection to model

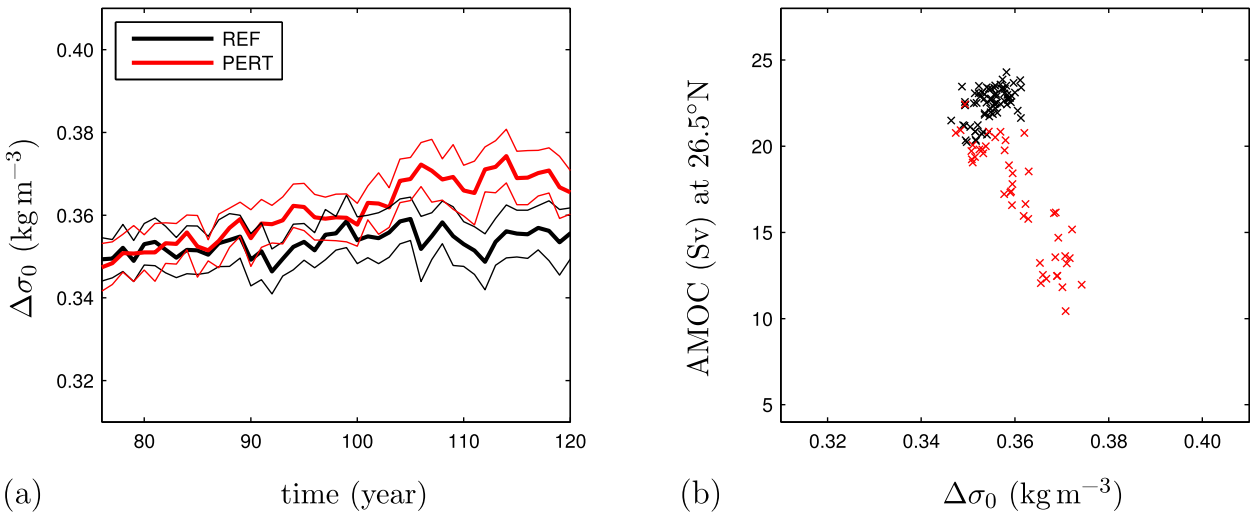

FIG. 5. As in Fig. 4, but for the $R_{0.1}$ configuration.

years 76 and 116 of the PERT simulation (Figs. 6a,b), for which daily averaged output is available.

In nonstationary simulations isopycnal transport is not necessarily equal to diapycnal transport (Marsh et al. 2000). In addition to the isopycnal streamfunction ψ, one also needs to consider the change in time of

$$V(\phi, b, t) = r_0^2 \int_{\phi}^{90^\circ} \cos\phi' \int_{\lambda_W}^{\lambda_E} \int_{-H}^{\zeta(\lambda,\phi,b,t)} dz\, d\lambda\, d\phi', \quad (3)$$

the volume north of the section at latitude ϕ, and below the surface with buoyancy b (Figs. 6c,d). A transformation "pseudo" streamfunction

$$G(\phi, b, t) = \psi(\phi, b, t) + \frac{\partial V(\phi, b, t)}{\partial t} \quad (4)$$

can then be defined (Figs. 6e,f), which has the useful property that its derivative with respect to latitude $\partial G/\partial\phi$ gives the correct diapycnal flux of waters at latitude ϕ. Its derivative with respect to b, however, includes both the isopycnal component of the transport and the rate of volume change of waters with buoyancy between b and $b + \delta b$, north of ϕ. In addition, G will not be zero at the southern boundary of a closed basin if changes in V are nonzero; it is hence not a streamfunction in the nondivergent sense. So, the two streamfunctions ψ and G are complementary; the first provides the correct isopycnal transport below the surface with buoyancy b, and the second provides the diapycnal transport north of latitude ϕ.

In year 76, the inflation and deflation of layers only represents a relatively small contribution to the isopycnal flow, especially for potential densities exceeding 36.5 kg m^{-3} (Fig. 6c). Hence, the isopycnal (Fig. 6a) and transformation (Fig. 6e) streamfunctions are similar, providing a picture of a coherent pole-to-pole circulation, having a maximum of about 23 Sv at 53°N and $\sigma_2 = 36.7$ kg m^{-3}. The near-vertical contours between 60° and 65°N reflect the corridor associated with diapycnal transformation and the sinking of water to deeper layers in the Labrador Sea. The local maximum at 71°N reflects overturning in the Nordic seas. The relatively flat contours south and "below" the location of maximum overturning represent southward flow, which is of the same magnitude throughout the Atlantic, indicating that diffusion-driven diapycnal flow is relatively unimportant in the Atlantic basin.

The difference between year 116 and year 76 of the transformation streamfunction (Fig. 6f) indicates that the diapycnal transport north of 53°N weakens by about 18 Sv. This suggests that during the PERT experiment less and less water has access to the adiabatic pathway as a result of less isopycnals being shared between the Southern Ocean and northern North Atlantic, consistent with the reduction of buoyancy loss and ventilation rates over this area (Weijer et al. 2012). The changes in convective activity between year 116 and year 76 are also reflected in the decrease of the maximum mixed layer density, shown as the gray lines in Figs. 6e and 6f.

The isopycnal transport is also reduced, weakening by about 15 Sv at 53°N, but only by about 10 Sv at the southern margin of the Atlantic (Fig. 6b). The difference between the change in isopycnal and diapycnal transports indicates a change in the inflation and deflation of layers of equal potential density (Fig. 6d), which is not accounted for by the adiabatic pole-to-pole framework (Wolfe and Cessi 2009, 2011) in which steady-state

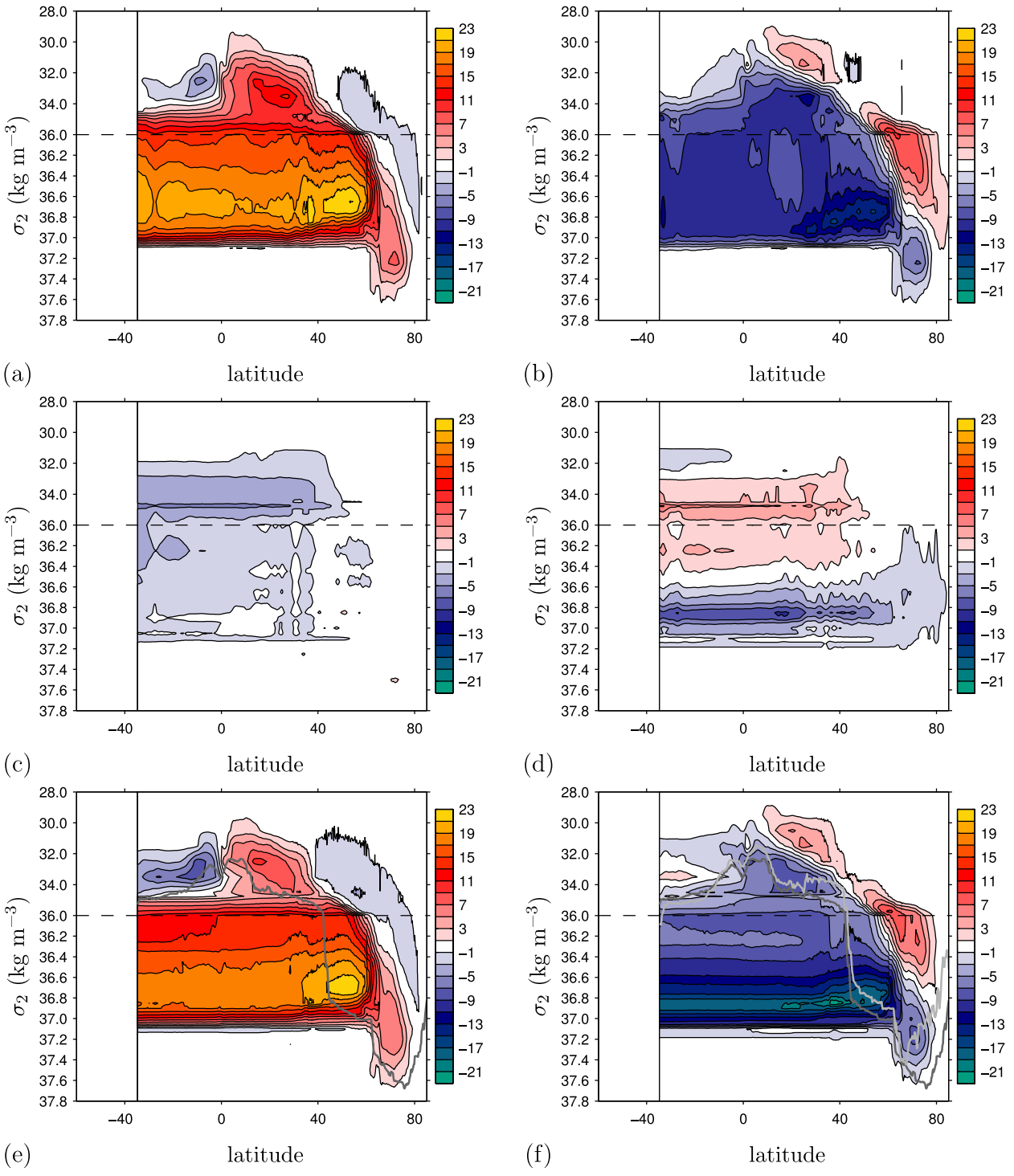

FIG. 6. Annual-mean isopycnal and diapycnal transports in the Atlantic (contour interval 2 Sv) for the $R_{0.1}$ configuration. (left) Year 76 of PERT and (right) the difference between year 116 and year 76. Note the change in the vertical scale at $\sigma_2 = 36.0\,\mathrm{kg\,m^{-3}}$ in (a)–(f) (a),(b) Isopycnal streamfunction ψ. (c),(d) Volume tendency $\partial V/\partial t$. (e),(f) Transformation streamfunction G, overlain with the year-round maximum density of the mixed layer in the Atlantic sector, shown in dark gray for year 76 and light gray for year 116 [only in (f)].

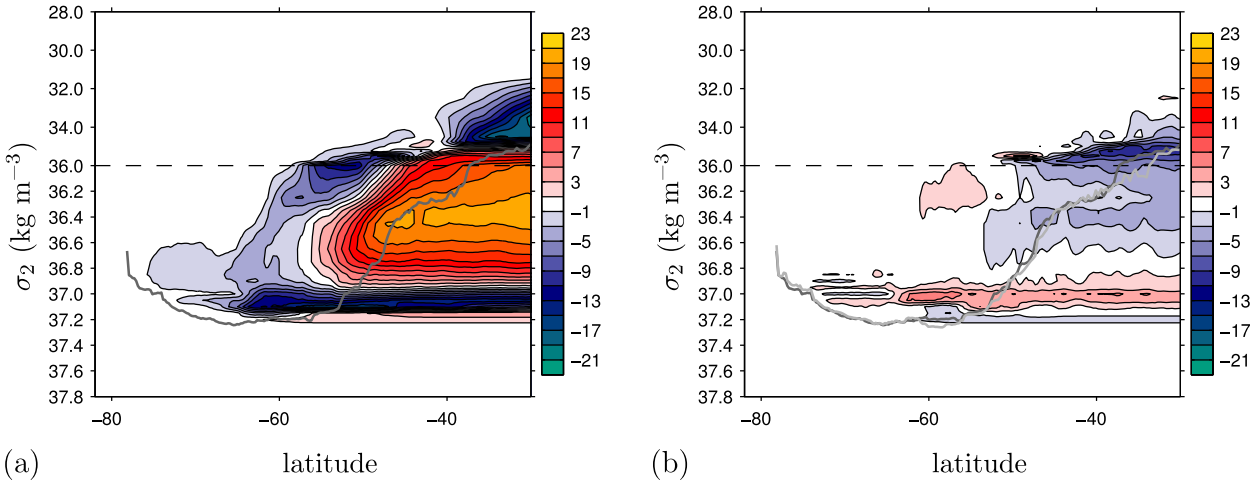

FIG. 7. Global South Pole–referenced transformation streamfunction G' (contour interval 2 Sv), with the (a) results for year 76 of PERT and the (b) difference between year 116 and year 76. As discussed in the text, G' shows the transport relative to $\phi = 90°$S. The dark and light gray lines indicate the year-round, global maximum density of the mixed layer in years 76 and 116, respectively.

conditions are assumed. Despite the reduction in distance between levels of equal potential density with $37.23 > \sigma_2 > 36.9\,\mathrm{kg\,m^{-3}}$, there is no change in diffusion-driven diapycnal transport in this density range within the duration of the experiment (Fig. 6f). On the other hand, the upwelling through the isopycnal surfaces around $\sigma_2 = 36.7\,\mathrm{kg\,m^{-3}}$, occurring in the North Atlantic subtropical gyre, is slightly weakened, which appears compatible with the local inflation of density layers.

It turns out that the net reduction of the transformation of light to dense waters in the Atlantic is not accompanied by a reduction of dense to light transformation outside the Atlantic. In Fig. 7 we plot the global, South Pole–referenced transformation streamfunction G', which is defined in a similar way as G [Eq. (4)], except that it is zero at $\phi = 90°$S, rather than at $\phi = 90°$N. It shows that in year 76 (Fig. 7a) there is an "upward" cross-isopycnal transport of about 20 Sv (and a "downward" transport of 4 Sv) through the $\sigma_2 = 36.7\,\mathrm{kg\,m^{-3}}$ surface in the region south of where the Atlantic is confined by continents (34°S). In year 116, there is no change in the dense to light transformation through this isopycnal surface (Fig. 7b). For latitudes north of 34°S, the difference between year 116 and year 76 of the global transformation streamfunction (not shown) is not significantly different from that calculated for the Atlantic (Fig. 6f), indicating that the changes in diapycnal transport in the Pacific are small. In fact, in a globally integrated sense, the reduction of North Atlantic dense water formation causes a decrease of the volume of dense waters, which is accommodated primarily within the Atlantic (Fig. 6d), but involving the other basins as well.

As suggested recently by Wolfe and Cessi (2009, 2011), water mass transformation theory can be used to relate the steady-state strength of the adiabatic, interhemispheric (pole to pole) overturning circulation to the surface density distribution. This is achieved by incorporating the idea that Southern Ocean Ekman transport can maintain a deep overturning circulation in the absence of diapycnal mixing (Toggweiler and Samuels 1995). The main suggestion is that a pole-to-pole circulation exists, because the following two conditions are met: 1) westerlies are present over the Southern Ocean, which drive a thermally indirect meridional flow and establish a deep stratification; and 2) there is a set of outcropping isopycnals that are shared between the Southern Ocean and the northern North Atlantic, providing a deep, adiabatic pathway for the southward return flow of North Atlantic Deep Water. The theory can be extended by including a diabatic abyssal overturning cell, corresponding to Antarctic Bottom Water (Nikurashin and Vallis 2011, 2012). While being a very useful concept in equilibrium flows, it thus appears that, over the time scale of the experiments considered here, the concept of the adiabatic pole-to-pole circulation is only of limited value in quantitatively relating local changes in buoyancy forcing to (remote) modifications of the basin-scale overturning circulation.

5. Evolution of the Atlantic salinity budget

We next turn to the main element of the paper, that is, the relation between the AMOC strength and the basinwide freshwater transport and in particular on the role of M_{ov} as an indicator of the salt advection feedback.

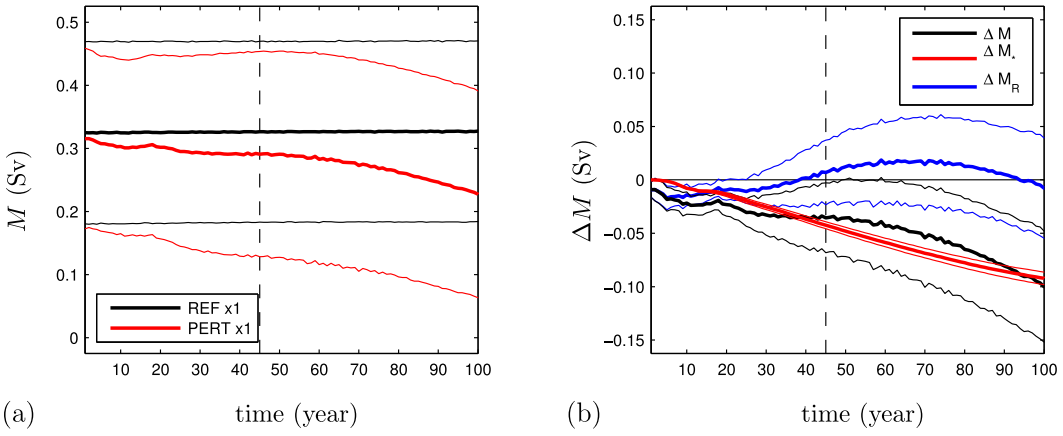

FIG. 8. (a) Net advective contribution to the freshwater budget M [Eq. (8)] for the $x1$ configuration for REF and PERT. (b) The quantity ΔM (black), the difference between REF and PERT of net advection of freshwater presented in (a). This difference is decomposed into a contribution ΔM_* (red) due to the advection of the salinity of REF (S^{REF}) by the difference zonally integrated velocity ($\Delta\Phi_{34°\mathrm{S}}$) and a remainder ΔM_R(blue).

For POP, the freshwater budget is obtained by multiplying the salinity S equation by $-1/S_0$, where $S_0 = 35$ psu is a reference salinity, and integrating the result over the Atlantic and Arctic basins. Written in short, the result is

$$\mathrm{EPR} = Q_t + M + R. \tag{5}$$

The left-hand side of this equation is the total evaporation minus precipitation and runoff (EPR):

$$\mathrm{EPR} = \frac{r_0^2}{S_0}\iint_A F_S \cos\phi \, d\lambda \, d\phi, \tag{6}$$

calculated as the integral of the virtual salt flux F_S (positive for a flux corresponding to evaporation) across the surface of the Atlantic and Arctic (subscript A). The first term on the right-hand side of Eq. (5) represents the change in time of the freshwater content:

$$Q_t = \frac{r_0^2}{S_0}\frac{d}{dt}\iint_A \left(\int_{-H}^{0} S\, dz + \eta S_1\right)\cos\phi \, d\lambda \, d\phi, \tag{7}$$

where H is the depth of the ocean, S_1 is the upper-layer salinity, and η is the free surface elevation. The second term on the right-hand side of Eq. (5) is net advection of freshwater:

$$M = \frac{-r_0}{S_0}\iint_{\mathrm{BS}} vS\cos\phi \, dz \, d\lambda + \frac{-r_0}{S_0}\iint_{34°\mathrm{S}} vS\cos\phi \, dz \, d\lambda, \tag{8}$$

consisting of contributions due to advection across Bering Strait (subscript BS) and the section between South America and South Africa at 34°S, respectively. Parameterized subgrid-scale transports are captured by the last term in Eq. (5), which is denoted by R because it is not calculated explicitly, but diagnosed as the residual in the freshwater equation.

For the $x1$ configuration, the mean value of EPR equals 0.37 Sv in REF and is −0.13 Sv in PERT, as expected. The mean value of Q_t in the REF simulation is about 5×10^{-3} Sv, indicating that the integrated freshwater budget is close to steady state. In the PERT experiment, $Q_t > -0.5$ Sv (not shown), meaning that the overall freshening of the basin is smaller than what is expected solely from the freshwater perturbation. The main reason for this is that M decreases in time (Fig. 8a). In REF, the mean value of M is 0.33 Sv, while in PERT its annual-mean values decrease to 0.29 Sv after 45 yr and further to 0.23 Sv after 100 yr. The implication is that the change in M in the PERT simulation partly offsets the original perturbation. The residual term is relatively small (the mean value of R in REF is 0.03 Sv) and is only modestly affected by the freshwater perturbation (not shown).

In the following, let Δ denote a difference between PERT and REF, such that for a variable X, $\Delta X = X^{\mathrm{PERT}} - X^{\mathrm{REF}}$. Noting that $\Delta M < 0$ arises due to differences between PERT and REF in the velocity and salinity fields at Bering Strait and at the section at 34°S, the question is to what degree ΔM can be attributed to the change in overturning strength at 34°S. To analyze this issue, some further notation needs to be introduced. First, let $\hat{f}$ denote the section average of a function $f(\lambda, \phi, z, t)$ at $\phi = 34°\mathrm{S}$:

$$\hat{f} = \left(\int_{34°\mathrm{S}} dz\, d\lambda\right)^{-1}\int_{34°\mathrm{S}} f\, dz\, d\lambda. \tag{9}$$

Second, we use $\langle f \rangle$ to indicate the zonal mean of f:

$$\langle f \rangle(z) = \left(\int_{\lambda_W}^{\lambda_E} d\lambda \right)^{-1} \int_{\lambda_W}^{\lambda_E} f \, d\lambda \,, \tag{10}$$

where the integral is evaluated at $\phi = 34°\text{S}$. Finally, the divergence-free transport per unit depth is defined as

$$\Phi_{34°\text{S}}(z) = r_0 \cos\phi \int_{\lambda_W}^{\lambda_E} \langle v \rangle(z) - \hat{v} \, d\lambda \,, \tag{11}$$

again evaluated at $\phi = 34°\text{S}$. Note that the integral over depth of $\Phi_{34°\text{S}}$ vanishes, so that $\Phi_{34°\text{S}}$ is only associated with net tracer transport if the zonal-mean tracer concentration varies with depth. Because the section-integrated transport in the Atlantic Ocean is relatively small (about 1 Sv) compared to the AMOC (Ψ) as defined in Eq. (1), $\Phi_{34°\text{S}}$ is roughly equal to the negative of the vertical derivative of Ψ at 34°S.

We now identify the part of ΔM that is associated with changes in the AMOC strength with

$$\Delta M_* = \int_{-H}^{0} -\Delta\Phi_{34°\text{S}}(z) \times \frac{\langle S^{\text{REF}} \rangle(z)}{S_0} dz \,, \tag{12}$$

and denote the remainder by $\Delta M_R = \Delta M - \Delta M_*$. Based on this decomposition, it appears that the reduction of M in PERT can to a large degree be attributed to the change in AMOC strength, since the annual-mean values of ΔM_R are relatively small (Fig. 8b).

As suggested by Huisman et al. (2010), ΔM_* can be related to a characteristic of the unperturbed reference simulation, because

$$\Delta\Phi_{34°\text{S}}(z) \approx -\xi(t) \Phi^{\text{REF}}_{34°\text{S}}(z) \,, \tag{13}$$

with some $\xi(t) > 0$ being a function of time only. This relation also appears to hold true for the experiments described here (not shown). As a result, $\Delta M_* \approx -\xi(t) \, M^{\text{REF}}_{\text{ov}}$, where

$$M_{\text{ov}} = \frac{-r_0}{S_0} \int_{34°\text{S}} (\langle v \rangle - \hat{v}) \langle S \rangle \cos\phi \, dz \, d\lambda \tag{14}$$

is the freshwater transport associated with the AMOC. The mean value of M_{ov} in the REF simulation equals 0.14 Sv. The fact that it is positive is hence consistent with ΔM_* being negative.

We continue by investigating whether the salt advection feedback has a similar signature in the $R_{0.1}$ configuration. In the REF run the net evaporation across the Atlantic and Arctic basins (EPR) is about 0.32 Sv (Fig. 9a). As expected, EPR is about 0.5 Sv smaller in the PERT simulation, but it also shows gradual changes in time that can be attributed to the response of evaporation to temperature changes. In contrast to the $x1$ case, the effect of advection on the freshwater balance appears to be similar in both experiments (Fig. 9b). Possibly, there is a difference in M between PERT and REF, but if so, it is entirely masked by interannual variability. The freshwater tendency Q_t varies around zero in the unperturbed case, but roughly equals −0.5 Sv in the PERT experiment (Fig. 9c). For the $R_{0.1}$ configuration, the advective salt fluxes were not saved during run time. Therefore, M is calculated from monthly-averaged model output, which means that the contribution due to within-month variations of v and S is neglected. The resulting errors are part of the residual R. However, its mean value is small in both REF and PERT (Fig. 9d). In addition, the typical variations of R are similar in the two experiments. So, this analysis shows that the extra freshwater input in PERT is totally compensated by storage within the Atlantic and Arctic basins.

To evaluate the significance of the AMOC reduction in PERT for the net advection of freshwater, we apply the same decomposition as in the above, $\Delta M = \Delta M_* + \Delta M_R$ (Fig. 10a). The variability in ΔM is clearly dominated by the remainder ΔM_R, and it has an amplitude that is significantly stronger than the mean of the AMOC contribution ΔM_*. The latter is of comparable magnitude as in the $x1$ case, but of opposite sign during most of the simulation, despite the fact that the forcing is similar in the two configurations. This means that the effect of the AMOC, if any, is to enhance the original freshwater perturbation. It should be noted that in the upper part of the water column $\langle S^{\text{REF}} \rangle(z)$ is slightly increasing in time. At the surface, its annual-mean value increases by about 0.1 psu over the course of the simulation. However, this has hardly any impact on the evolution of ΔM_*; almost the same result is obtained when using the simulation-mean value of $\langle S^{\text{REF}} \rangle(z)$ rather than monthly averages.

According to the theory proposed by Huisman et al. (2010), the fact that ΔM_* is positive during most of the simulation should be reflected in M_{ov} being negative for the REF simulation. However, as illustrated in Fig. 10b, a complication arises because M_{ov} is evolving over the course of the REF simulation. It is positive at the start of the run, but decreases to values around and below zero. This change occurs despite the absence of a clear trend in the AMOC strength at 34°S (Fig. 3b). If, instead of using monthly averages for $\langle S^{\text{REF}} \rangle(z)$, the simulation-mean value of $\langle S^{\text{REF}} \rangle(z)$ is used in the equation for M_{ov}

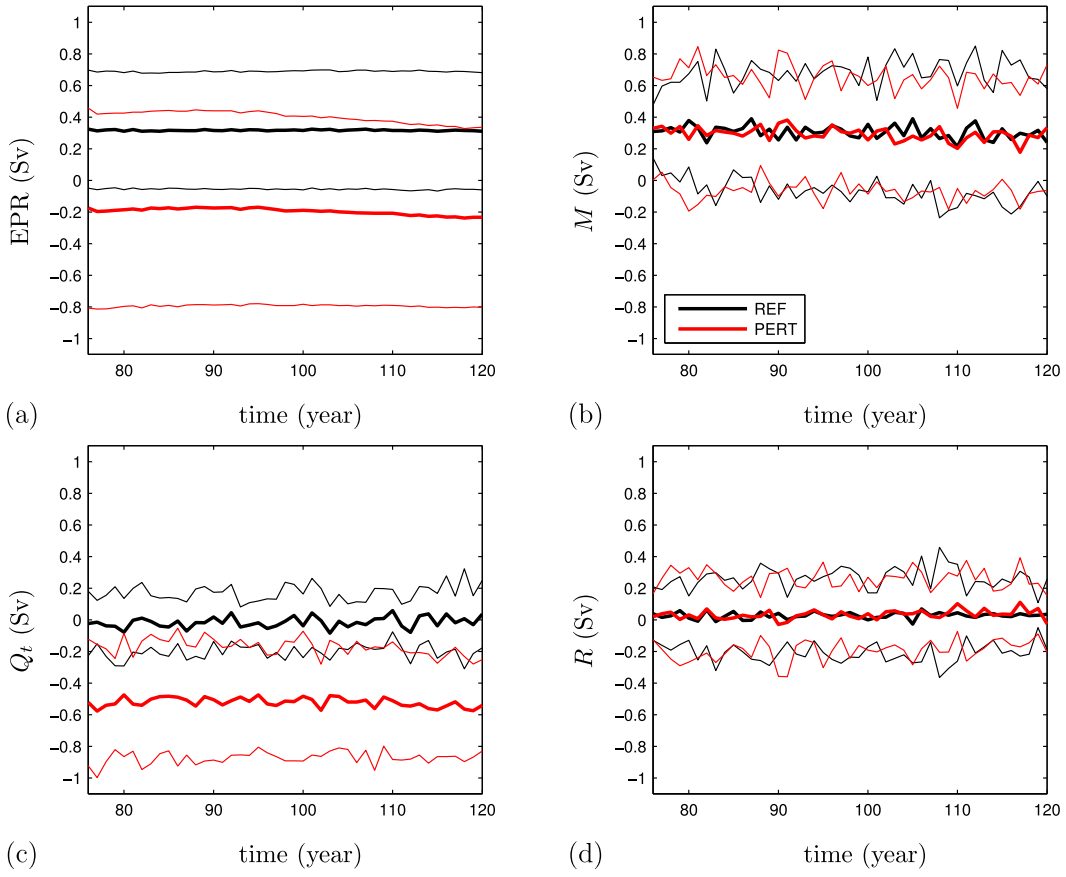

FIG. 9. Contributions to the freshwater budget expressed by Eq. (5) for the $R_{0.1}$ configuration for REF and PERT: (a) EPR, (b) M, (c) Q_t, and (d) R.

[Eq. (14)], the result is almost constant in time and has a mean of 0.023 Sv, which is positive rather than negative. Whereas the increase in upper-ocean salinities hardly influenced the evolution of ΔM_*, they are the main reason for the decrease of $M_{\rm ov}^{\rm REF}$. These results imply that in the $R_{0.1}$ configuration, $\Delta\Phi_{34^\circ{\rm S}}(z)$ is not simply proportional to $\Phi_{34^\circ{\rm S}}^{\rm REF}(z)$. In other words, the relation expressed by Eq. (13), which is an important element

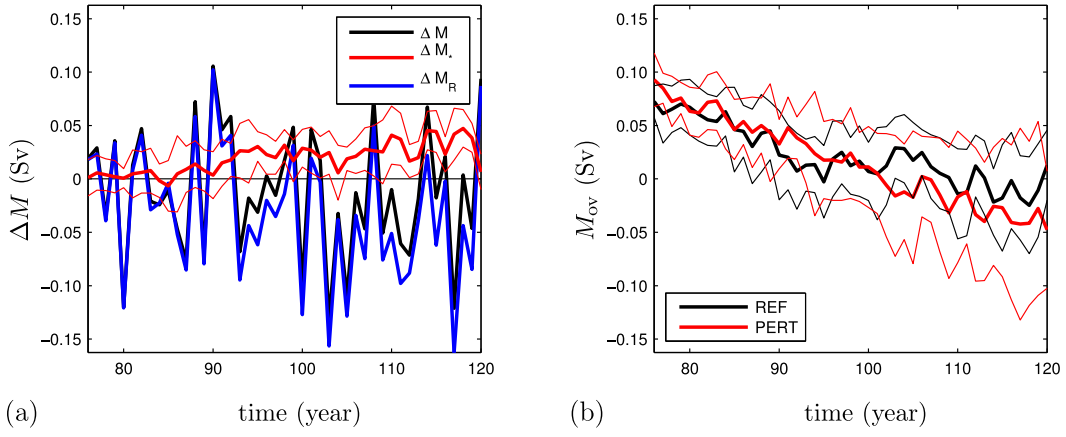

FIG. 10. (a) As in Fig. 8b, but for the $R_{0.1}$ configuration. For the black and blue lines, the thin lines indicating the 1-yr root-mean-square deviation are omitted to avoid overloading the figure. (b) Overturning freshwater transport as in Eq. (14) for REF and PERT.

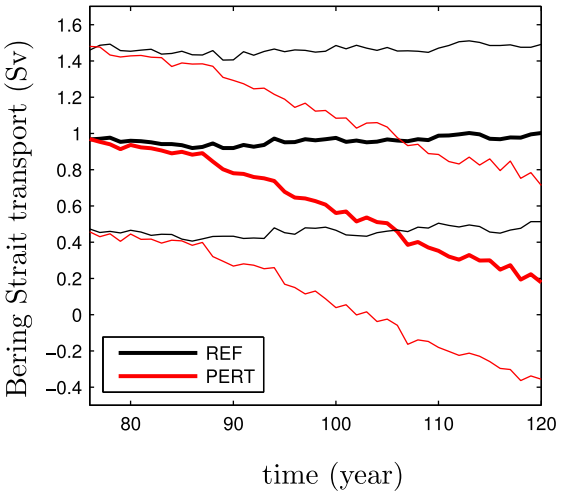

FIG. 11. Northward transport through Bering Strait for the $R_{0.1}$ configuration for REF and PERT.

of the theory that supports the relevance of M_{ov} as a stability indicator, does not hold.

In the PERT simulation, the change in upper-ocean salinities is even stronger than in REF, with surface values of $\langle S^{PERT} \rangle$ increasing by about 0.2 psu. This effect is more important than the reduction of the AMOC, which is reflected by ΔM_*, as discussed above. As a result, the reduction of M_{ov} in PERT is stronger than in REF. The conclusion regarding the fact that $\Delta M_{ov} < 0$ is hence somewhat counterintuitive: whereas the total effect of M_{ov} is to partly offset the original freshwater perturbation, this is due to the change in the zonal-mean salinity profile, rather than the result of the reduction of the AMOC.

The impact of the freshwater perturbation is not limited to the overturning component of the zonally integrated circulation, but also affects the section-integrated horizontal transport. Because long-term tendencies of area-integrated sea surface height (SSH) are negligible compared to the section-integrated transport, its annual-mean value is nearly independent of latitude and hence equal to the annual-mean transport through Bering Strait (Fig. 11). The reduction of the Bering Strait transport in PERT is caused by an increase in SSH in the Arctic (not shown), which leads to a reduction of the pressure gradient across the strait. As in Hu et al. (2012), the changes in the SSH field result from dynamic processes that occur in response to the freshwater perturbation, which by itself does not represent a source of additional volume, as it is implemented as a virtual salt flux.

The divergence of freshwater advection associated with the section-integrated transport is given by (Drijfhout et al. 2011)

$$M_{\Delta BS} = \frac{-r_0}{S_0} \int_{BS} vS \cos\phi \, dz \, d\lambda + \frac{-r_0}{S_0} \int_{34°S} \hat{v}\hat{S} \cos\phi \, dz \, d\lambda . \tag{15}$$

Figure 12a shows that the within-year root-mean-square deviations of $M_{\Delta BS}$ are much stronger than its annual-mean values, so that care must be taken in interpreting the difference between the two simulations. Because short-term changes in the salinity field are small (relative to S_0), the large intra-annual variability is mainly caused by the variations in the Bering Strait transport (Fig. 11) and the sectionwide transport at 34°S, which are not fully correlated to each other on the time scale of 1 month. Because an imbalance between the two transports cannot persist indefinitely (a difference of 1 Sv roughly corresponds a sea level change of 1 mm day^{-1} in the Atlantic basin), the interannual variability of $M_{\Delta BS}$ is much smaller than the within-year variability. In the REF

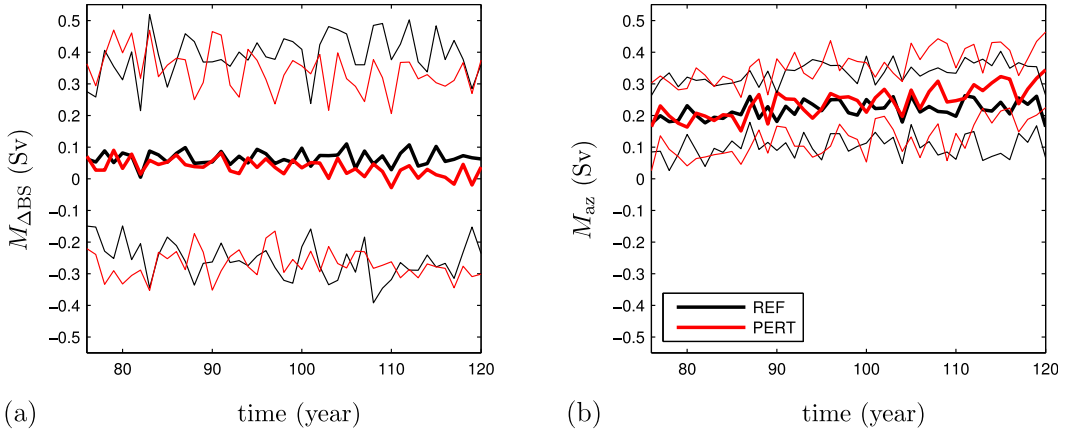

FIG. 12. Net freshwater advection (a) associated with the section-integrated transport [Eq. (15)] and (b) due to zonal variations of velocity and salinity [Eq. (17)] for REF and PERT.

simulation, there appears to be no indication of changes on the time scale of the experiment. The mean value of $M_{\Delta BS}$ in REF is 0.07 Sv, roughly consistent with a mean section-integrated transport of 0.96 Sv and a mean salinity contrast between Bering Strait and 34°S of 2.8 psu. In contrast to the results for M_{ov}, the evolution of $M_{\Delta BS}$ is consistent with what is expected from the change of the velocity structure. The long-term reduction of Bering Strait transport (Fig. 11) in PERT indeed causes less freshwater to be deposited in the Atlantic; although the effect can only be distinguished from the interannual variability toward the end of the simulation (Fig. 12a). As in the results of Hu et al. (2012), the response of the sectionwide transport to the enhanced GrIS melting thus appears to oppose the freshening induced directly by the perturbation.

So far, we have discussed two contributions to the net advection of freshwater M [Eq. (8)]. As detailed in Drijfhout et al. (2011), a third contribution can be defined (denoted by M_{az}), which is related to zonal variations of velocity and salinity that arise from the gyre circulation and eddies, such that

$$M = M_{ov} + M_{\Delta BS} + M_{az}. \tag{16}$$

Here, the expressions for the contributions are given, respectively, by Eqs. (14), (15), and by

$$M_{az} = \frac{-r_0}{S_0} \int_{34°S} v' S' \cos\phi \, dz \, d\lambda, \tag{17}$$

where we used $f' = f - \langle f \rangle$ to denote the deviation from the zonal mean of a function f. The changes of $M_{\Delta BS}$ in PERT and of M_{ov} both in REF and PERT, occurring over the course of the integration, are of comparable magnitude to the typical interannual variations of the total advective freshwater convergence M (Fig. 9b). Consistent with the finding that M seems to be constant in both experiments, Fig. 12b suggests (at least for PERT) that M_{az} is increasing in time to compensate for the decrease of the other two contributions. Compared to the long-term change, however, the interannual variability of M_{az} is rather strong. As a consequence, we have been unable to find a satisfactory explanation for this result, which should link the evolution of M_{az} to changes in the zonal structure of the velocity and salinity field at 34°S.

6. Summary and discussion

We presented results from two 45-yr simulations of the strongly eddying global POP model, one reference simulation (REF) and one simulation in which an extreme, integrated freshwater perturbation of 0.5 Sv due to Greenland Ice Sheet melting was prescribed (PERT). For comparison, results from a corresponding set of simulations with POP configured at low horizontal resolution were provided. The two versions of the model show a quantitatively similar response of the basinwide circulation to the freshwater perturbation. Our objective was to compare the signature of the salt advection feedback between the two configurations. Although this feedback is of secondary importance for the evolution of the AMOC in these short-duration experiments, because of the large amplitude of the forcing its expression could still be studied. Clearly, the simulations should not be considered as a realistic scenario for present-day climate change, for which a 0.1-Sv perturbation would already be seen as catastrophic. However, 0.5 Sv may be considered as an upper bound of the total freshwater input associated with a typical Heinrich event during the last glacial period (Roche et al. 2004).

The salt advection feedback is thought to be responsible for a strong sensitivity of the ocean to freshwater forcing and may lead to abrupt transitions due to the existence of multiple steady states (Bryan 1986; Rahmstorf 1996, 2000). One of the simplest representations of the salt advection feedback is provided by the two-box model of Stommel (1961), which suggests that the following three conditions are important for the feedback to operate: 1) the large-scale flow is proportional to a meridional density gradient; 2) the large-scale flow carries heat and freshwater, affecting that density gradient; and 3) the boundary conditions are such that temperature anomalies are damped out much quicker than salinity anomalies, so that the flow has a stronger control over the salinity gradient than over the temperature gradient. In this paper, we framed the presentation of the results around the first two of these conditions.

Although counterexamples have been provided (De Boer et al. 2010), there are several results from coarse-resolution models that indicate that the strength of the AMOC is proportional to the north–south difference in density (Rahmstorf 1996; Dijkstra 2008) or pressure (Griesel and Maqueda 2006). In agreement with these studies and condition 1, a positive correlation between annual-mean values of the AMOC strength and the potential density contrast ($\Delta\sigma_0$) was established for the $x1$ configuration. However, in the $R_{0.1}$ version of the model, the correlation was found to be weak and of opposite sign.

The $R_{0.1}$ results were further analyzed using water mass transformation theory. In the PERT experiment the density range with outcropping isopycnals is reduced in the North Atlantic, both directly due to the enhanced runoff from Greenland, but also as a result of the

shallowing of the mixed layer and the associated weakening of buoyancy loss in the Labrador Sea. As a result, the rate of light to dense transformation is strongly reduced in the region around 60°N (Fig. 6f). However, the local change in diapycnal transport does not correspond quantitatively to the change in isopycnal flow at other latitudes in the Atlantic (Fig. 6b). This is explained by the fact that, over the time scale of the experiment, no compensating reduction in dense to light transformation is established elsewhere in ocean. As a result, the amount of dense water is continuously decreasing, both inside and outside the Atlantic. Although eventually a new quasi equilibrium could be reached under sustained freshwater forcing, none of the results presented show a sign of leveling off at the end of the 45-yr integration.

Through comparison of the $x1$ and the $R_{0.1}$ simulations, we found that the changes in the basinwide circulation lead to a different response in net advective freshwater convergence in the Atlantic basin. In the $x1$ configuration, the results appeared to be consistent with condition 2, as illustrated in Fig. 8. In addition, we found support that M_{ov}, which is positive in these experiments, is a relevant indicator of the stability of the AMOC, in accordance with the conclusions of Rahmstorf (1996) and Huisman et al. (2010). In the strongly eddying model, on the other hand, the effect of the AMOC on the freshwater budget was found to be small compared to typical interannual variations in the total net advection of freshwater (Figs. 9 and 10). Furthermore, the effect appeared inconsistent with the sign of the stability indicator M_{ov}. In addition to M_{ov}, we found that the net freshwater advection is determined by the contribution associated with the section-integrated transport ($M_{\Delta BS}$) and that due to zonal variations in salinity and velocity (M_{az}). However, we were unable to establish a functional relationship between these contributions and the freshwater perturbation.

In the simulations described here, and in Weijer et al. (2012), sea surface salinity is not restored to climatology, allowing the circulation to have a stronger impact on salinity than on temperature. The sea surface temperature (SST) field is not fixed, though. This means that, since bulk formulae are used to calculate evaporation, the surface freshwater flux may respond to changes in the circulation. This effect is indeed observed in the $R_{0.1}$ PERT experiment (Fig. 9a). Results from another coarse-resolution model suggest that atmospheric feedbacks modify the sensitivity of the circulation to freshwater perturbations only quantitatively (Den Toom et al. 2012). If, however, the basin-scale salt advection feedback is insignificant in eddying models, feedbacks operating through atmospheric processes could be relatively important for the behavior of the coupled ocean–atmosphere system. It may therefore be necessary to incorporate a dynamical atmosphere to accurately assess climate system response to a strong freshwater anomaly from Greenland. Similarly, the incorporation of a dynamical ice model might lead to qualitatively different results than presented here.

From the ocean-only simulations as carried out here with the different versions of the POP model, we conclude that the response of the Atlantic Ocean circulation to freshwater perturbations differs in an important aspect: the transient net freshwater advection by the overturning at the southern boundary of the Atlantic, which forms a central element in the salt advection feedback (Huisman et al. 2010), has an opposite sign in the low- and high-resolution versions of the model. This may have far-reaching consequences regarding the value of stability indicators based on the Atlantic freshwater budget (De Vries and Weber 2005; Huisman et al. 2010; Drijfhout et al. 2011), the existence of a multiple equilibria regime of the AMOC (Rahmstorf 1996), and the theories of rapid climate transitions in the past (Alley et al. 2003).

Acknowledgments. This work was supported in part by the Earth System Modeling and Regional and Global Climate Modeling programs of the Office of Biological and Environmental Research within the U.S. Department of Energy's Office of Science. The computations were done on the Huygens IBM Power6 at SARA in Amsterdam, on the Institutional Computing facilities at Los Alamos National Laboratory, and on the Jaguar supercomputer at the National Center for Computational Sciences at Oak Ridge National Laboratory. Use of the SARA computing facilities was sponsored by the National Computing Facilities Foundation (NCF) under the Project SH084-11 with financial support from the Netherlands Organization for Scientific Research (NWO). Research for MdT was supported by a NWO Toptalent Grant. EvS was supported by the Australian Research Council. We thank three anonymous reviewers for suggesting substantial improvements to the manuscript.

REFERENCES

Alley, R. B., and Coauthors, 2003: Abrupt climate change. *Science,* **299,** 2005–2010, doi:10.1126/science.1081056.

Andersson, A., K. Fennig, C. Klepp, S. Bakan, H. Graßl, and J. Schulz, 2010: The Hamburg Ocean Atmosphere Parameters and Fluxes from Satellite Data—HOAPS-3. *Earth Syst. Sci. Data Discuss.,* **3,** 143–194, doi:10.5194/essdd-3-143-2010.

Bower, A. S., M. S. Lozier, S. F. Gary, and C. W. Boning, 2009: Interior pathways of the North Atlantic meridional overturning circulation. *Nature,* **459,** 243–247, doi:10.1038/nature07979.

Bryan, F. O., 1986: High-latitude salinity effects and interhemispheric thermohaline circulations. *Nature,* **323,** 301–304, doi:10.1038/323301a0.

Bryden, H. L., B. A. King, and G. D. McCarthy, 2011: South Atlantic overturning circulation at 24°S. *J. Mar. Res.,* **69,** 38–55, doi:10.1357/002224011798147633.

Cunningham, S. A., and Coauthors, 2007: Temporal variability of the Atlantic meridional overturning circulation at 26.5°N. *Science,* **317,** 935–938, doi:10.1126/science.1141304.

De Boer, A. M., A. Gnanadesikan, N. R. Edwards, and A. J. Watson, 2010: Meridional density gradients do not control the Atlantic overturning circulation. *J. Phys. Oceanogr.,* **40,** 368–380.

Den Toom, M., H. A. Dijkstra, A. A. Cimatoribus, and S. S. Drijfhout, 2012: Effect of atmospheric feedbacks on the stability of the Atlantic meridional overturning circulation. *J. Climate,* **25,** 4081–4096.

De Vries, P., and S. L. Weber, 2005: The Atlantic freshwater budget as a diagnostic for the existence of a stable shut down of the meridional overturning circulation. *Geophys. Res. Lett.,* **32,** L09606, doi:10.1029/2004GL021450.

Dijkstra, H. A., 2007: Characterization of the multiple equilibria regime in a global ocean model. *Tellus,* **59A,** 695–705, doi:10.1111/j.1600-0870.2007.00267.x.

——, 2008: Scaling of the Atlantic meridional overturning in a global ocean model. *Tellus,* **60A,** 749–760, doi:10.1111/j.1600-0870.2008.00326.x.

Drijfhout, S. S., E. Maier-Reimer, and U. Mikolajewicz, 1996: Tracing the conveyor belt in the Hamburg large-scale geostrophic ocean general circulation model. *J. Geophys. Res.,* **101** (C10), 22 563–22 575.

——, S. Weber, and E. van der Swaluw, 2011: The stability of the MOC as diagnosed from model projections for pre-industrial, present and future climates. *Climate Dyn.,* **37,** 1575–1586, doi:10.1007/s00382-010-0930-z.

Dukowicz, J. K., and R. D. Smith, 1994: Implicit free-surface method for the Bryan-Cox-Semtner ocean model. *J. Geophys. Res.,* **99** (C4), 7991–8014, doi:10.1029/93JC03455.

Fekete, B. M., C. J. Vörösmarty, and W. Grabs, 2000: Global composite runoff fields based on observed river and simulated water balances. Global Runoff Data Centre Tech. Rep. 22, 108 pp.

Gerdes, R., W. Hurlin, and S. Griffies, 2006: Sensitivity of a global ocean model to increased run-off from Greenland. *Ocean Modell.,* **12,** 416–435, doi:10.1016/j.ocemod.2005.08.003.

Griesel, A., and M. Maqueda, 2006: The relation of meridional pressure gradients to North Atlantic Deep Water volume transport in an ocean general circulation model. *Climate Dyn.,* **26,** 781–799, doi:10.1007/s00382-006-0122-z.

Hawkins, E., R. S. Smith, L. C. Allison, J. M. Gregory, T. J. Woollings, H. Pohlmann, and B. de Cuevas, 2011: Bistability of the Atlantic overturning circulation in a global climate model and links to ocean freshwater transport. *Geophys. Res. Lett.,* **38,** L10605, doi:10.1029/2011GL047208.

Hu, A., G. A. Meehl, W. Han, and J. Yin, 2009: Transient response of the MOC and climate to potential melting of the Greenland Ice Sheet in the 21st century. *Geophys. Res. Lett.,* **36,** L10707, doi:10.1029/2009GL037998.

——, and Coauthors, 2012: Role of the Bering Strait on the hysteresis of the ocean conveyor belt circulation and glacial climate stability. *Proc. Natl. Acad. Sci. USA,* **109,** 6417–6422, doi:10.1073/pnas.1116014109.

Huisman, S. E., M. den Toom, H. A. Dijkstra, and S. Drijfhout, 2010: An indicator of the multiple equilibria regime of the Atlantic meridional overturning circulation. *J. Phys. Oceanogr.,* **40,** 551–567.

Hurrell, J. W., J. J. Hack, D. Shea, J. M. Caron, and J. Rosinski, 2008: A new sea surface temperature and sea ice boundary dataset for the community atmosphere model. *J. Climate,* **21,** 5145–5153.

Jungclaus, J. H., H. Haak, M. Esch, E. Roeckner, and J. Marotzke, 2006: Will Greenland melting halt the thermohaline circulation? *Geophys. Res. Lett.,* **33,** L17708, doi:10.1029/2006GL026815.

Large, W. G., and S. Yeager, 2004: Diurnal to decadal global forcing for ocean and sea-ice models: The data sets and flux climatologies. National Center for Atmospheric Research Tech. Rep. NCAR/TN-460+STR, 112 pp.

Maltrud, M., F. Bryan, and S. Peacock, 2010: Boundary impulse response functions in a century-long eddying global ocean simulation. *Environ. Fluid Mech.,* **10,** 275–295, doi:10.1007/s10652-009-9154-3.

Marsh, R., A. Nurser, A. Megann, and A. New, 2000: Water mass transformation in the Southern Ocean of a global isopycnal coordinate GCM. *J. Phys. Oceanogr.,* **30,** 1013–1045.

——, D. Desbruyeres, J. L. Bamber, B. A. de Cuevas, A. C. Coward, and Y. Aksenov, 2010: Short-term impacts of enhanced Greenland freshwater fluxes in an eddy-permitting ocean model. *Ocean Sci.,* **6,** 749–760, doi:10.5194/os-6-749-2010.

Mernild, S. H., G. E. Liston, C. A. Hiemstra, and J. H. Christensen, 2010: Greenland Ice Sheet surface mass-balance modeling in a 131-yr perspective, 1950–2080. *J. Hydrometeor.,* **11,** 3–25.

Murray, R. J., 1996: Explicit generation of orthogonal grids for ocean models. *J. Comput. Phys.,* **126,** 251–273.

Nikurashin, M., and G. Vallis, 2011: A theory of deep stratification and overturning circulation in the ocean. *J. Phys. Oceanogr.,* **41,** 485–502.

——, and ——, 2012: A theory of the interhemispheric meridional overturning circulation and associated stratification. *J. Phys. Oceanogr.,* **42,** 1652–1667.

Rahmstorf, S., 1996: On the freshwater forcing and transport of the Atlantic thermohaline circulation. *Climate Dyn.,* **12,** 799–811, doi:10.1007/s003820050144.

——, 2000: The thermohaline ocean circulation: A system with dangerous thresholds? *Climatic Change,* **46,** 247–256, doi:10.1023/A:1005648404783.

Rignot, E., and P. Kanagaratnam, 2006: Changes in the velocity structure of the Greenland Ice Sheet. *Science,* **311,** 986–990, doi:10.1126/science.1121381.

——, I. Velicogna, M. van den Broeke, A. Monaghan, and J. Lenaerts, 2011: Acceleration of the contribution of the Greenland and Antarctic Ice Sheets to sea level rise. *Geophys. Res. Lett.,* **38,** L05503, doi:10.1029/2011GL046583.

Roche, D., D. Paillard, and E. Cortijo, 2004: Constraints on the duration and freshwater release of Heinrich event 4 through isotope modelling. *Nature,* **432,** 379–382, doi:10.1038/nature03059.

Stammer, D., 2008: Response of the global ocean to Greenland and Antarctic ice melting. *J. Geophys. Res.,* **113,** C06022, doi:10.1029/2006JC004079.

Stommel, H., 1961: Thermohaline convection with two stable regimes of flow. *Tellus,* **13,** 244–230, doi:10.1111/j.2153-3490.1961.tb00079.x.

Toggweiler, J. R., and B. Samuels, 1995: Effect of Drake Passage on the global thermohaline circulation. *Deep-Sea Res.,* **42,** 477–500, doi:10.1016/0967-0637(95)00012-U.

Walin, G., 1982: On the relation between sea-surface heat flow and thermal circulation in the ocean. *Tellus,* **34,** 187–195, doi:10.1111/j.2153-3490.1982.tb01806.x.

Weijer, W., W. P. M. De Ruijter, H. A. Dijkstra, and P. J. Van Leeuwen, 1999: Impact of interbasin exchange on the Atlantic overturning circulation. *J. Phys. Oceanogr.,* **29,** 2266–2284.

——, M. E. Maltrud, M. W. Hecht, H. A. Dijkstra, and M. A. Kliphuis, 2012: Response of the Atlantic Ocean circulation to Greenland Ice Sheet melting in a strongly-eddying ocean model. *Geophys. Res. Lett.,* **39,** L09606, doi:10.1029/2012GL051611.

Wolfe, C. L., and P. Cessi, 2009: Overturning circulation in an eddy-resolving model: The effect of the pole-to-pole temperature gradient. *J. Phys. Oceanogr.,* **39,** 125–142.

——, and ——, 2011: The adiabatic pole-to-pole overturning circulation. *J. Phys. Oceanogr.,* **41,** 1795–1810.

Zhang, R., 2010: Latitudinal dependence of Atlantic meridional overturning circulation (AMOC) variations. *Geophys. Res. Lett.,* **37,** L16703, doi:10.1029/2010GL044474.